Innovation of Chemistry & Materials for Sustainability
Volume 3, Issue 1, Jan.- June **2026**
RESEARCH ARTICLE
ISSN (Print): 3049 – 2548
ISSN (Online): 3049 – 0146

Towards Sustainability: Fiber Architectural, Interfacial Behaviorism, and Topographical Relationship in Sisal Fiber Reinforced Butadiene Rubber Composites for Commodity Rubber Goods

Souvik Das[a], Himon Sen[b], Payel Dasgupta[c], Vivek K. Yadav[b], Narayan Ch. Das[b]*, and Debasish Das[a]*

[a]Department of Jute and Fiber Technology, University of Calcutta, Kolkata, 700019, India.
[b]Rubber Technology Centre, Indian Institute of Technology Kharagpur, Kharagpur, West Bengal, 721302, India.
[c]Agricultural and Food Engineering Department, Indian Institute of Technology Kharagpur, Kharagpur, West Bengal, 721302, India.
*Correspondence: ncdas@rtc.iitkgp.ac.in (N. Ch. Das); ddjf@caluniv.ac.in (D. Das)

Abstract: Researchers are increasingly using biocomposites in engineering to reduce their environmental impact, with cellulosic fibers as the primary natural fiber source. These fibers and their composites offer many benefits but also have drawbacks, especially regarding environmental factors. For the first time, the study examined the reinforcing effects of short sisal fibers (4.0-5.5 mm) in butadiene rubber (BR). These fibers were combined with the BR matrix and vulcanized to create flexible composite sheets. Standard techniques, such as tensile testing, hardness (Shore A) measurements, water absorption behavior, Payne effect study, abrasion resistance study, aspect ratio study, and swelling behavior, were used to assess the physico-mechanical properties. The $BRSF_{30}$ composite demonstrated substantial enhancements in mechanical properties, with tensile strength increasing by 306.02%, hardness (Shore A) rising by 32%, and modulus of toughness improving by 45.28% compared to the pristine ($BRSF_0$). Notably, the final decomposition temperature of $BRSF_{30}$ also increased by 3.28% relative to the pristine compound ($BRSF_0$). Morphological studies of cryofactured composites using scanning electron microscopy (SEM) provided detailed insights into fiber-matrix interactions and fiber pull-out at the fractured surfaces, while atomic force microscopy (AFM) demonstrated superior dispersion of the fibers in $BRSF_{30}$ composite compared to $BRSF_0$ and $BRSF_{50}$. Fourier transform infrared spectroscopy (FTIR) was used to analyze chemical structure variations in samples. Efficient crosslinking in $BRSF_{30}$ creates a 3D network within the rubber matrix, reducing polymer chain mobility and limiting moisture ingress to 6.05%. The crosslink density of $BRSF_{30}$ increased by 67.11% compared to the pristine compound ($BRSF_0$). Additionally, the rubber process analyzer (RPA) illustrated the Payne effect within the composites, showing a decrease in storage modulus with increasing strain amplitude. The $BRSF_{30}$ composite showed a reduction in abrasion volume loss of approximately 50.41% and an increase in abrasion resistance of about 102% compared to the pristine compound. The $BRSF_{30}$ composite exhibited an optimal aspect ratio of 15.94±0.02, and the soil burial and environmental durability test showed negligible weight loss and no significant color change over 15 days. The newly developed sisal fiber–BR composite may have potential applications as commodity rubber goods.

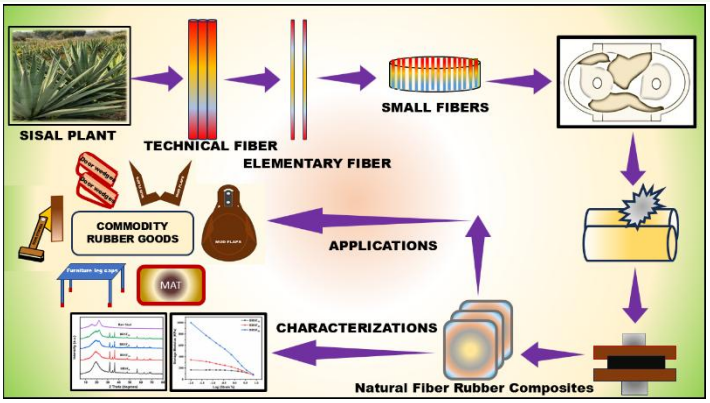

Keywords: *Environmental impact, biocomposites, sisal fiber, butadiene rubber, matrix*

1. Introduction

The development of biocomposites in the composites sector has garnered considerable attention nowadays. In the production of biocomposite materials that address both economic and environmental challenges, natural fibers are becoming increasingly significant as reinforcing fibers. Natural fibers, in contrast to synthetic fibers, lack the established scientific and technological foundation necessary to reliably provide regulated performance suitable for engineering applications.[1] The requirement for precise and trustworthy natural fiber characteristics rises in this context. Synthetic fiber-reinforced polymer composites are utilized in a wide range of industrial sectors, including civil engineering, automotive, aerospace, sports, recreation, and leisure, among others. These fiber composites offer superior mechanical properties and are more resistant to environmental aging; however, they pose hazards to people and the environment. The most widely used synthetic fibers with excellent mechanical properties are glass and carbon fibers; however, they produce more carbon dioxide and greenhouse gas emissions. When these synthetic, non-biodegradable fibers are disposed of in landfills, they seriously pollute the environment.[2] Hence, nowadays, researchers are reinforcing polymer-based composites with natural fibers. Natural fibers are an excellent substitute due to their low density, biodegradability, strong flexural and tensile strength, minimal carbon dioxide emissions, and good acoustic and thermal insulation properties. These fibers are effective reinforcing components in the production of polymer composites, making them beneficial for various lightweight industrial uses. Natural fiber-reinforced composites face several challenges, including poor modulus, fiber delamination, significant water absorption, and limited applicability in high-load-bearing situations.[3] Various natural fibers, such as ramie, banana, pineapple, and sisal, are combined with different polymer resin matrices. Among them, sisal fiber-reinforced polymer composites exhibit notable mechanical improvements due to their higher cellulose content, which contributes to superior tensile strength compared to other natural fiber composites. Plant-based cellulosic fibers such as flax, hemp, and ramie are increasingly considered sustainable substitutes for synthetic fibers in medium-strength and advanced composites, primarily because they are renewable, affordable, biodegradable, and possess exceptional tensile properties.[4] Sisal fiber, derived from the leaves of the sisal plant, stands out for its mechanical and physicochemical properties, as well as its socioeconomic importance.[5] The composition of sisal fiber includes 68-72% cellulose, 10-12% hemicellulose and pectins, 8-10% water, 2-3% waxes, 9-10% lignin, and 1-2% soluble components.[6]

Butadiene rubber (BR), also known as polybutadiene, is another significant material characterized by excellent flexibility and abrasion resistance. Its durability makes it suitable for high-impact applications, allowing it to maintain its shape even under stress. The use of fillers, which enhance specific properties of composites, has shown promise in improving the characteristics of BR. There is growing interest in the potential of natural organic fillers to improve the mechanical and fire resistance properties of polymer composites. BR can serve as a matrix for various cellulosic and lignocellulosic

https://doi.org/10.63654/icms.2026.03055
Innov. Chem. Mater. Sustain. **2026**, *3*(1), 55-69
Received: 14 April 2026; Revised: 24 May 2026; Accepted: 27 May 2026; Published (online): 30 May 2026

Table 1. *The specifications of the materials used in this study.*

Materials	Functions	Manufacturer
Butadiene rubber (BR), CISAMER 1220, ML_{1+4}@ 100 °C = 45, cis content 96%	Matrix	Reliance Industries Pvt. Ltd. (Navi Mumbai, India)
Toluene (purity~99.0 percent)	Solvent for dissolving the unvulcanized compound	Merck, India
Sulfur (purity~98.0 percent)	Curative	Nice Chemicals Pvt. Ltd., India
Stearic acid (purity~99.0 percent)	Activator for curing	Godrej Soap Ltd., Chennai, India
TBBS (N-tert-butyl-2-benzothiazyl sulfenamide) (purity~98.0 percent)	Delayed-action accelerator	National Organic Chemicals Industries Ltd., India.
CTP (N-(Cyclohexylthio) phthalimide) (purity~98.0 percent)	Pre-vulcanization inhibitor or scorch retarder	National Organic Chemicals Industries Ltd., India.
Zinc Oxide (purity~98.0 percent)	Activator	Merk, India
6PPD (N-(1,3-Dimethylbutyl)-N'-phenyl-p-phenylenediamine) (purity~99.0 percent)	Antiozonant	National Organic Chemicals Industries Ltd., India.
TQ (Polymerized 2,2,4-trimethyl-1,2-dihydroquinoline) (purity~99.0 percent)	Antioxidant	National Organic Chemicals Industries Ltd., India.

fiber composites obtained from plant sources, where the physico-mechanical properties of these composites are heavily influenced by the interfacial adhesion between the natural fibers and BR.[7] When the interaction is insufficient, it may be necessary to modify the fiber surface through chemical or physical treatments. Techniques such as NaOH treatment, stearic acid treatment, Maleic anhydride polypropylene (MAPP) treatment, silane treatment, and Maleic anhydride polyethylene (MAPE) treatment have been documented in literature as effective methods for enhancing fiber-matrix adhesion.[8,9]

Organic fiber-reinforced composites are the subject of extensive research due to their non-abrasive and recyclable properties. These fibers are recognized as economical, renewable, and recyclable resources that are readily accessible worldwide and exhibit excellent mechanical properties. Fibrous cellulosic fillers have attracted significant interest recently, as they have been shown to enhance the mechanical performance of composites more effectively than non-fibrous fillers. The performance of fiber-reinforced composites is influenced by several factors, including fiber-matrix interactions, fiber volume fraction, fiber aspect ratio, fiber orientation, and the efficiency of stress transfer at the fiber-matrix interface.[10] Notable studies, including those by Shekeil and his colleagues, on his evaluation of the mechanical characteristics of date palm-reinforced nitrile butadiene rubber composite for biobased materials, found the maximum tensile strength and hardness of 2.06 MPa and 70, respectively, for 30 wt % fiber loading in the composite.[11] Venkatesan and Bhaskar focused on using specific testing methods to evaluate and contrast the distinct mechanical properties exhibited by the abaca-sisal composite material.[12] Paran and his co-workers reported the thermal and mechanical properties of nitrile butadiene rubber containing organoclay and rice straw natural fibers, and green thermoplastic elastomer vulcanizate nanocomposites, and reported that the NPCRS40 composite has final degradation temperatures below 520 ºC.[13] Das and his colleagues previously studied and reported the effect of adding sisal fiber to carboxylated nitrile butadiene rubber composites.[14] This work innovatively combines BR and natural fibers to create a hybrid architecture and evaluates its mechanical, thermal, morphological, surface topography, aspect ratio, crosslink density, abrasion, soil burial, and environmental durability studies. The findings from this study aim to drive the development of economical, superior-performance, and ecologically friendly materials that benefit next-generation composite materials for commodity rubber goods and the advanced manufacturing industry.

2. Experimental Section

2.1 Materials

The materials used in the current investigation, particularly for manufacturing purposes, include sisal fiber as reinforcement and BR which serves as the matrix. The sisal fibers were obtained from farmers cultivating sisal in Odisha, India. Table 1 lists the specifications of the materials utilized in this investigation.

The sisal fibers underwent a meticulous cleaning process using water to eliminate contaminants. Subsequently, the cleaned fibers were sun-dried for 72 hours, followed by an additional drying phase in a hot-air oven at 50 ℃ for 24 hours. To safeguard against moisture, the dried fibers were stored in polythene bags. Using a Universal Testing Machine (Model: H50KS, United Kingdom), the characteristics of the sisal fiber were assessed as per ASTM D3822 standards. Table 2 represents the tensile characteristics of sisal fiber. The fibers were measured using digital vernier calipers to determine the lengths to be used in the tensile test. The results include the average from ten measurements, with the standard deviation included in parentheses.

Table 2. *Tensile characteristics of the raw fiber.*

Average length (in mm) of the Raw Sisal Fiber	Average diameter (in µm) of the Raw Sisal Fiber	Tensile Strength (in Megapascals)	Percent Strain at Yield Point	Yield force (in Newton)
50.00 (± 0.60)	285.93 (± 4.31)	235.50 (±18.20)	20.01 (± 4.01)	3.20 (± 0.31)

2.2 Sisal Fiber's Average Diameter and Length Employed for Manufacturing the Composites

The study involved the manual chopping of long sisal fibers to produce shorter fibers ranging from 4.00 to 5.50 mm, which were randomly mixed to fabricate the composites. The average diameter of the raw sisal fiber, measured using an Optical Image Analyzer (Model Name: Leica DMLM, Germany) and analyzed with ImageJ software, was approximately 285.93 ± 4.31 micrometers for ten different samples, at two different points throughout its length, as shown in Table 3 and Figure 1(a-e). Additionally, the lengths of fifty randomly selected manually chopped fibers were measured using digital vernier calipers, yielding an average length of 5.00 ± 0.20 mm as shown in Table 3 and Figure 1(a-e).

2.3 Preparation of Sisal Fiber-BR Composites

The Haake Rheomix® laboratory internal mixer was used to prepare rubber composites by blending fibers with butadiene rubber (Cobalt catalyst) and other rubber additives for ten minutes at 50°C and 60 rpm. After softening BR in the internal mixer for 2 minutes, chopped sisal fiber was gradually added, and the mixture was run for 5 minutes under the same working conditions. This temperature effectively softens and plasticizes the rubber, facilitating improved mixing and fiber dispersion. After that, zinc oxide (ZnO) and stearic acid were added, followed by the addition of 6PPD and TQ as a

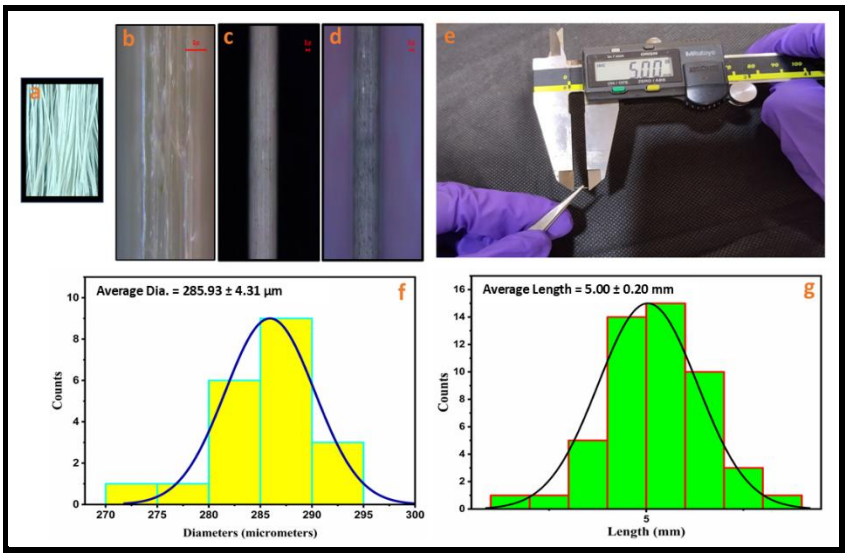

Figure 1. *(a) Chopped sisal fibers used in this study, (b,d) Raw sisal fiber images from the optical microscope in the bright-field and (c) dark field, (e) Sisal fiber length measurement using vernier callipers, (f) Average diameter of raw sisal fibers used for preparing the composites, (g) Average length of raw sisal fibers used for fabricating the composites.*

weather-resistant additive, for one minute at 50°C and 60 rpm. A delayed-action accelerator, TBBS (N-tert-butyl-2-benzothiazyl sulfenamide), along with CTP (N-(Cyclohexylthio) phthalimide), a pre-vulcanization inhibitor or scorch retarder, was mixed into the internal mixer for one minute at 50°C and 60 rpm. Finally, Sulphur was added as a curative and mixed at room temperature. And finally, the compounded product from the Haake internal mixer was passed through a laboratory-scale two-roll mill for two minutes. Throughout the entire mixing procedure, very minimal heat buildup was observed. Additional information on mixing methods is available in Table 4 and Figure S1 of the supporting information. The mold was then shielded from moisture and air and kept at 25°C for six hours. A moving die rheometer (MDR) (RHEO-LINE MDR, Prescott Instruments) was used to measure the composites' rheometric characteristics and curing time (t_{90}) at 160 °C. A hydraulic press (Moore Hydraulic Press, UK) was used to produce 2 mm-thick rubber sheets by compression molding at this temperature. Compression time varied among samples according to the t_{90} (optimum cure time) values reported in Table S1 in the supporting information.

Table 3. *The raw fibers' average length and diameter utilized for preparing the composites.*

Average length (in millimeters)	Average diameter (in micrometers)
5.00 ± 0.20	285.93 ± 4.31

Table 5 lists the names of the composites developed from Sisal fiber and BR, with varying fiber loadings. The composite's fiber content has been changed from 0 to 50 phr (parts per hundred rubber). The composites were classified as $BRSF_Y$, with BR standing for butadiene rubber, SF for sisal fiber, and Y for sisal fiber content (which ranged from 0 to 50 phr).

Table 4. *The compounding recipe for the developed sisal fiber-BR composites..*

Compounding Stages	Compounding Conditions at Haake Rheomix
Softening of BR (Cobalt catalyst)	Performed the operation for two minutes at 50 degrees Celsius with a rotor speed of 60 rpm.
Addition of Sisal Fibers (Chopped)	Run the rotor at 60 revolutions per minute for five minutes at 50 degrees Celsius.
Addition of ZnO + Stearic Acid	Run the rotor at 60 revolutions per minute for one minute at 50 degrees Celsius.
Addition of 6 PPD + TQ	Run the rotor at 60 revolutions per minute for one minute at 50 degrees Celsius.
Addition of TBBS + CTP	Run the rotor at 60 revolutions per minute for one minute at 50 degrees Celsius.
Addition of the Curatives (Sulfur)	Adding in two roll mills at room temperature for two minutes.

3. Characterizations of the Materials

A dry atmosphere was employed for the storage of $BRSF_Y$ composites for two days preceding analysis. The Sigma 300 VP-FESEM (Zeiss, Germany) was used to obtain micrographs of the composites at an accelerating voltage of 5 kV across various magnifications. Cryo-fractured composites were secured onto stubs with double-sided tape, followed by the sputtering of conductive gold particles using a vacuum evaporator. Scanning Electron Microscopy (SEM) facilitated the examination of fiber size and dispersion within the rubber matrix. Furthermore, morphological properties of both raw sisal fibers and those extracted post-dissolutions into toluene were assessed. A brief overview of the fiber extraction process is available in the supporting information. The Rubber Processing Analyzer (RPA) (Montech D-RPA 3000, Germany) was employed to evaluate

Table 5. *Fabrication of sisal fiber-BR composite based on 100 phr.*

Composites	Ingredients (phr)								
	BR	Sisal Fiber (Chopped)	ZnO	Stearic Acid	6PPD	TQ	TBBS	CTP	Sulfur
$BRSF_0$	100	0	5	2	1	2	1.2	0.30	2
$BRSF_{10}$	100	10	5	2	1	2	1.2	0.30	2
$BRSF_{30}$	100	30	5	2	1	2	1.2	0.30	2
$BRSF_{50}$	100	50	5	2	1	2	1.2	0.30	2

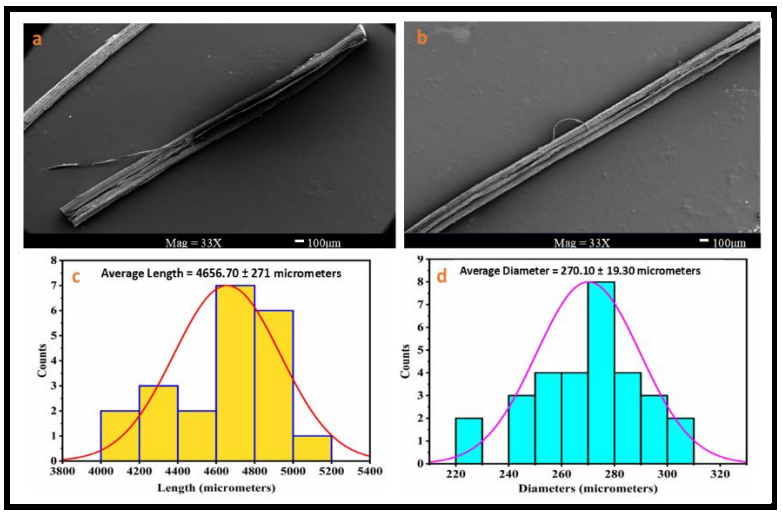

Figure 2. *The SEM micrographs of the raw fibers (a-b) with average length (c) and average diameter (d).*

the storage modulus of the sisal fiber BR composites during dynamic loading, facilitating the analysis of the "Payne effect" in the rubber composites. The following were the RPA test parameters: strain range 0.01–7 degrees, frequency 1 Hz, and temperature 70 °C. The chemical interactions among the composite components were examined using Fourier-transform infrared (FTIR) spectroscopy. Surface topography of the composites was assessed using an Atomic Force Microscope (AFM, Model 5500) from Agilent Technologies, Inc., United States. The analysis used Picoview version 1.12 for data evaluation, while rendering was performed with Pico Image version 6.20. The analysis covered a 90 µm x 90 µm range in the x and y dimensions, with an 8 µm resolution in the z direction. A Thermo Fisher Scientific Instruments (Model: Nicolet-6700, USA) spectrophotometer was employed, with ten scans over the frequency range of 4000–400 cm^{-1} collected in attenuated total reflectance (ATR) mode for each sample. The study also examined the thermal degradation of composites with varying fiber loadings. Evaluations were conducted using a PerkinElmer Pyris Diamond thermogravimetric analyzer (TGA) in a controlled nitrogen atmosphere. The testing was performed at a heating rate of ten degrees Celsius per minute, spanning a temperature range from room temperature to 650°C, with a nitrogen flow rate of 50 mL/min. The diffraction spectra of fibers and their composites with Cu-Kα radiation were obtained using a Bruker AXS diffractometer (Model: D2 Phaser). The fiber samples and composites were tested at 22 °C and 50% relative humidity using a Tinius Olsen H50KS universal testing apparatus. The fibers were tested in tension using five samples with a gauge length of 40 mm at a test speed of 2 mm/min, in accordance with ASTM D3822. The mechanical behavior of the composites was assessed using at least five samples in compliance with ASTM D412. A twenty-five millimeter gauge length and a speed of five hundred millimeters per minute were used in the trials. In accordance with ASTM D2240 criteria, a durometer was used to assess the Shore A hardness of the sample. Water absorption of the composites over a specific time period was monitored in accordance with ASTM D570 standards. The test samples, measuring 3.55 mm wide, 12.80 mm deep, and 62.50 mm long, were immersed in distilled water at room temperature. Equation S1 from the supporting information was used to calculate the weight percentage increase of the composites. Using toluene as the solvent and the equilibrium swelling technique, the composites' cross-linking density (n) was determined. Cut, weighed, and immersed in a container containing 50 cc of toluene for three days were samples measuring 20 mm by 10 mm by 0.60 mm. After removing the samples from the solvent, they were rapidly dried using tissue paper. We determined the cross-linking density of the rubber using the Flory-Rehner equation (Equation S2 in the supporting information).[15] To determine the distribution of fiber lengths in the vulcanizate and assess the degree of fiber breaking during mixing, fibers were removed from uncured mixes to calculate the aspect ratio (Length/Diameter).[16] The abrasion test was conducted in accordance with ASTM 5963, using an abrasion test machine (Gibitre, Italy) at room temperature. The drum speed was set to 40 revolutions per minute (rpm), and a load of 10 Newtons (N) was applied. The sample dimensions used in the test were 15 mm in diameter and 10 mm in thickness, as shown in Figure 13(k). The specific gravity was measured using a densimeter (Wallace Densimeters, X22B, UK) at room temperature. The worn surfaces of all composites after abrasion were analyzed using an SEM (Sigma 300 VP, Zeiss, Germany). All tests were performed at room temperature and 50 percent humidity. As shown in Figure 13(g), the abrasion button for the pristine sample ($BRSF_0$) contained no fibers. In contrast, fiber bunches were present in the abrasion buttons of the samples, as illustrated in Figure 13(h) for $BRSF_{10}$, Figure 13(i) for $BRSF_{30}$, and Figure 13(j) for $BRSF_{50}$. Optical microscopy (Axio Observer, Zeiss, Germany) images of the worn surfaces of the buttons are shown in Figure 13(l-o). The composites, measuring 2x1cm, with initial weights of 0.16 gm, 0.16 gm, 0.13 gm, and 0.17 gm for $BRSF_{10}$, $BRSF_{30}$, $BRSF_{50}$, and $BRSF_0$ composites, were buried in soil at a depth of 15cm for 2 weeks to study their degradation, as reported previously by Rong-or and his co-workers,[17] with slight modifications. At 7-day intervals, the samples were retrieved, cleaned, visually examined for any color change, dried to a constant weight, and the weight loss was calculated using Equation S3 in the supporting information. The fabricated rectangular composite sheet ($BRSF_{30}$) with an initial weight of 16.63 gm was kept in an open atmosphere for 2 weeks, and changes in weight, color, and tensile strength were monitored to assess durability. All the experimental data were statistically analyzed to estimate the analysis of variance with the help of statistical software SPSS ver.25 (IBM Corporation, Armonk, USA). All the tests were performed in triplicate, and the results are displayed as mean ± standard deviation. Significant differences were tested using the Tukey post hoc test ($p < 0.05$).

4. Results and Discussion

4.1 Morphological Evaluation and Impact of Fiber Loading on Tensile Behavior and Microstructure of the Composites.

The Scanning Electron Microscope (SEM) is one of the most versatile and widely used analytical instruments in modern science and engineering. It is one of the most powerful tools for understanding the performance of natural fiber composites. According to Figure 2(c-d), raw sisal fibers have an average diameter of 270.10 ± 19.30 µm and an average length of 4656.70 ± 271 µm. Twenty-one samples were used to measure the length of the raw sisal fibers. Using ImageJ, the raw fiber diameter was determined from ten samples at three distinct locations in their SEM micrographs. According to SEM, the average diameter and length of twenty samples of sisal fiber in the BR matrix were 190.00 ± 13.60 µm and 2870.30 ± 14.80 µm, respectively, as shown in Figure 3(a-c). Mechanical stress and breakage during mixing result in thinner,

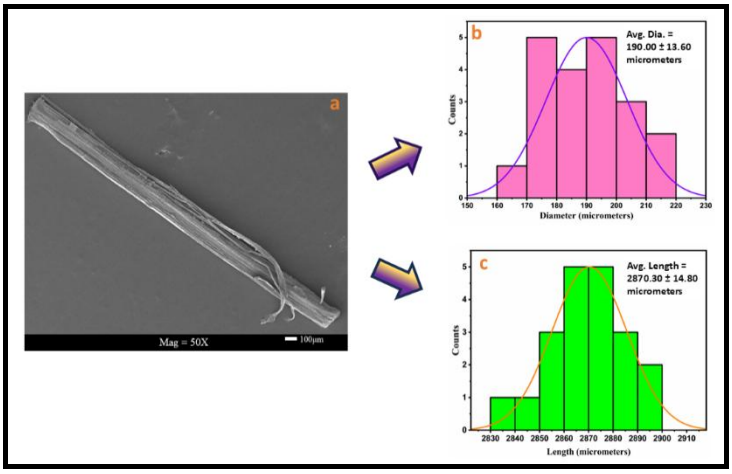

Figure 3. *The SEM micrographs of the raw sisal fiber in the BR matrix (a), with the average diameter (b) and average length (c).*

shorter fibers; the average fiber diameter in the rubber matrix was lower than that of the raw fibers. This fragmentation may be due to the mixer's large shearing force.[18]

SEM was used to analyze sisal fiber and gold-sputtered cryo-fractured composites. According to the findings, sisal fiber was heterogeneously distributed within the BR matrix. The outcomes of this study are displayed in Figure 2(a-b) and 4(a-c). Effective composites require the rubber and fiber surfaces to interact properly at the interfaces. Sisal fiber exhibits high polarity and hydrophilicity because of plenty of hydroxyl groups in its cellulose and lignin composition.[19] In contrast, BR is non-polar and hydrophobic, leading to significant thermodynamic incompatibility between the two materials and posing a challenge for effective reinforcement.[20] The reinforcement process is predominantly facilitated by mechanical interlocking rather than chemical adhesion, as only minimal physical attractions are present. The natural irregularities on the surface of sisal fibers facilitate BR engagement, allowing it to lock into the fiber's pits. Furthermore, during vulcanization, the rubber shrinks around the fiber, further enhancing the mechanical grip. The micrographs in Figure 4(a-c) provide visible evidence on how changing the fiber content in the BR matrix affects the composite's mechanical properties. We can link the increase in fiber density to the extent of the interfacial interaction and the resultant tensile behavior by examining the composites $BRSF_0$, $BRSF_{10}$, $BRSF_{30}$, and $BRSF_{50}$ with fiber loadings of 0, 10, 30, and 50 phr, respectively.

At a fiber loading of 10 phr, SEM images indicate an increased number of voids or air-trapped holes and notable "pull-out" sites, as shown in Figure 4(a). At this low fiber loading, there is a surplus of rubber matrix relative to the fibers. During mixing in a laboratory internal mixer, a low fiber volume results in insufficient internal shear stress to effectively interact with the rubber and the fiber surface. This results in very poor interfacial interactions.[21] The rubber matrix's inability to transmit stress to the fibers causes debonding. As a result, the $BRSF_{10}$ composite has the lowest tensile strength of 0.72±0.60 MPa, as shown in Figure 5 and Table 6. The substantial presence of air-trapped holes in the $BRSF_{10}$ composite facilitates fracture formation under stress, resulting in a decrease in tensile strength relative to $BRSF_0$. The fibers capable of bridging these holes are very few, leading to early failure of the material. At 30 phr fiber loading, due to increased fiber content in the rubber matrix, the SEM analysis reveals a reduced number of voids and the most uniform fiber dispersion within the matrix, as shown in Figure 4(b). Physical contact between the fiber and the rubber increased with increasing fiber in the composites. The fiber-rubber ratio was optimally adjusted in the composite material at 30 phr of fiber loading. Increasing fiber density from 10 to 30 phr increases the product's viscosity during mixing. The increased viscosity generates the requisite shear forces that push BR into the tiny pores of the sisal fibers, mechanically locking them in place. The matrix effectively transmits its load to the fibers compared to the $BRSF_{10}$ composite, yielding a tensile strength of 3.37±0.51 MPa, as shown in Figure 5

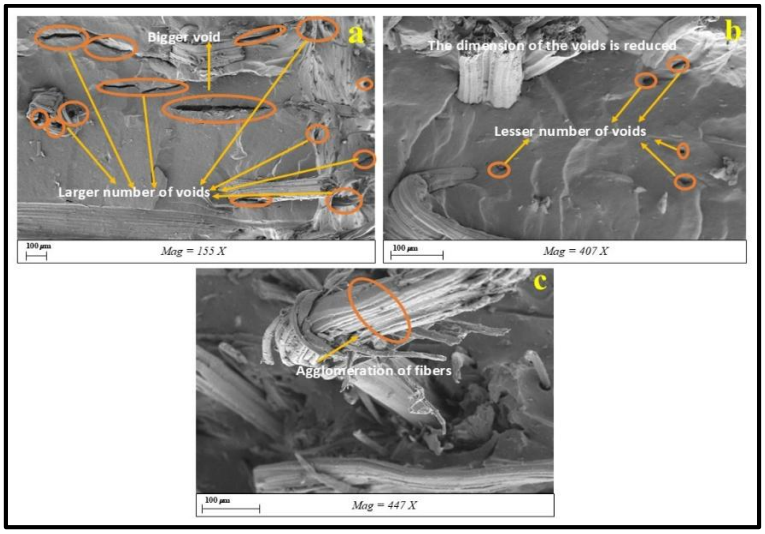

Figure 4. *The micrographs of the cryo-fractured composites (a) $BRSF_{10}$, (b) $BRSF_{30}$, (c) $BRSF_{50}$.*

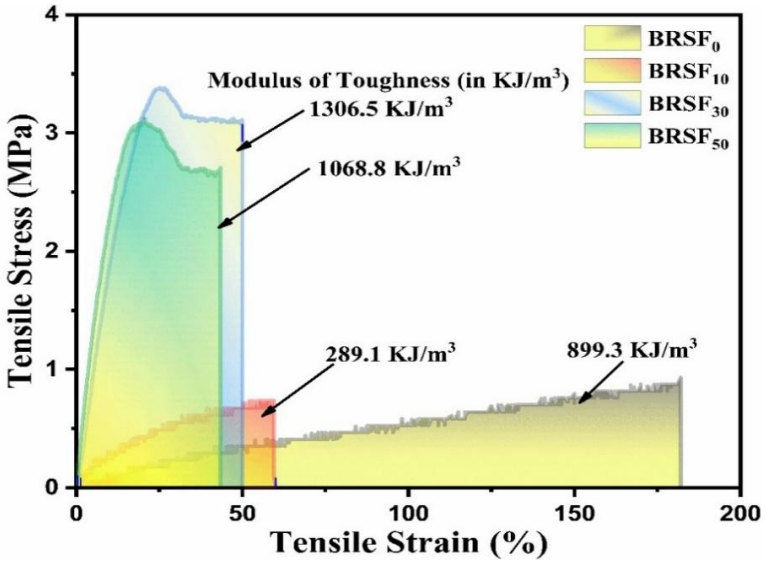

Figure 5. *Tensile plots with modulus of toughness (in KJ/m^3) of the fabricated sisal fiber reinforced BR composite of different fiber loadings.*

Table 6. *Tensile behavior of the composites with varying fiber loadings.*

Composites	Tensile Strength (MPa)	Hardness, Shore A	Modulus of Toughness (KJ/m^3)
BRSF$_0$	0.83±0.20^c	50.0±2^d	899.30±53.95^c
BRSF$_{10}$	0.72±0.60^d	61.5±1^c	289.10±11.56^d
BRSF$_{30}$	3.37±0.51^a	66.0±1^b	1306.50±78.33^a
BRSF$_{50}$	3.08±0.30^b	79.0±2^a	1068.80±95.12^b

All the data are represented in mean ± standard deviation. The different letters in the same column represent significant differences using Tukey's test (p <0.05).

and Table 6. The morphology of the BRSF$_{30}$ composite reveals fractured fibers rather than pulled-out fibers, suggesting that the interaction is more robust than that of the BRSF$_{10}$ composite. This results in optimal tensile performance, as shown in Figure 5. The negligible occurrence of voids was observed, yet effective transfer of stress from the matrix to the fibers remained.[22] At a fiber concentration of 50 phr, the SEM images reveal the highest fiber content, but they also show considerable fiber clumping, as shown in Figure 4(c). Although the overall fiber content in the rubber matrix has increased, the rubber volume was insufficient to fully encapsulate each fiber in the fabricated composite material. This leads to "fiber-to-fiber" rather than "fiber-to-rubber" interaction.[23] The agglomerates observed in the morphology study in Figure 4(c) function as internal flaws due to increased fiber concentration in the composite material. The tensile strength of the BRSF$_{50}$ composite is 3.08±0.30 MPa, which is inferior to that of the BRSF$_{30}$ composite but superior to that of the BRSF$_{10}$ composite, as observed in Figure 5 and Table 6. Although the agglomerates diminish the structural strength relative to the 30 phr sample, the substantial fiber content still provides greater overall reinforcement than the sparsely populated 10 phr composite. The inability of the agglomerates to evenly distribute the applied load limits the strength of the NBSF$_{50}$ composite. The modulus of toughness exhibits a pattern similar to that of the tensile strength study, as shown in Figure 5 and Table 6, with optimal performance observed in the 30 phr fiber-loaded composite, which can withstand significant stress without rapid fracture.[6,24]

4.2 Fiber-Matrix Interaction Study: Payne effect

The Payne effect was measured at 70°C during a strain sweep of an unvulcanized sample using the Montech D-RPA 3000, a rubber process analyzer (RPA) device. This was done to gain a better understanding of the interaction between rubber and filler. Lowering the Payne effect value (ΔG′) reflects a better rubber to filler interaction. The storage modulus and Payne effect (ΔG′) increase gradually as filler content increases,[25] as seen in Figure 6 and Table 7. The quantity of fiber clumping together increases with increasing sisal fiber content in the composite. The Payne effect and storage modulus of BRSF$_{50}$ are greater than those of BRSF$_{10}$ and BRSF$_{30}$, indicating that, in the composite with 50 phr fiber loading, there is little rubber-to-filler interaction and the highest fiber aggregation.[26] Although BRSF$_{10}$ has a lower Payne effect value, as observed in Figure 6 and Table 7, indicating better rubber-to-filler interaction, yet in section 4.1, the tensile results and morphology study indicate poor rubber-filler interaction and an uneven filler distribution. In BRSF$_{10}$, due to uneven fiber distribution, fibers do not form a network structure to withstand the stress on the composite. And that's why BRSF$_{10}$ shows lower mechanical strength than BRSF$_0$. In the case of BRSF$_{30}$, the Payne effect is greater than that of BRSF$_{10}$, but the rubber-to-filler interaction is superior to that of BRSF$_{10}$, as observed by the tensile value and morphology study. The best-balanced characteristics of BRSF$_{30}$ include optimal rubber-to-filler interaction and uniform fiber distribution. Because of its fiber network structure and uniform fiber distribution, BRSF$_{30}$ can withstand stress. On the other hand, BRSF$_{50}$ shows the highest degree of clumping of fibers (the highest storage modulus and Payne effect) and a poor fiber network; for this reason, it is not able to withstand stress like BRSF$_{30}$. A lower storage modulus for BRSF$_{10}$ indicates a weak fiber network and uneven fiber mixing. In contrast, a higher storage modulus for BRSF$_{50}$ indicates fiber aggregation due to increased filler-filler interaction rather than filler-rubber interaction, and hence, tensile strength was reduced compared to BRSF$_{30}$. However, BRSF$_{30}$ exhibits fiber networking, which is why the Payne effect and storage modulus fall between those of BRSF$_{10}$ and BRSF$_{50}$. Hence, BRSF$_{30}$ shows the best stress-bearing capacity compared to BRSF$_{10}$ and BRSF$_{50}$.[27,28]

Table 7. *Payne effect values of fabricated composites.*

Sample ID	Payne effect (MPa)(G' initial-G' final)
BRSF$_{10}$	85.26±5.11^c
BRSF$_{30}$	267.19±16.03^b
BRSF$_{50}$	912.4±54.74^a

All the data are represented in mean ± standard deviation. The different letters in the same column represent significant differences using Tukey's test (p <0.05).

4.3 FTIR Analysis

FTIR is primarily a tool for identifying chemical functional groups; it provides significant indirect evidence regarding the physical and mechanical interaction between the sisal fiber and the BR units. The unique patterns of the fiber spectrum in Figure 7 may

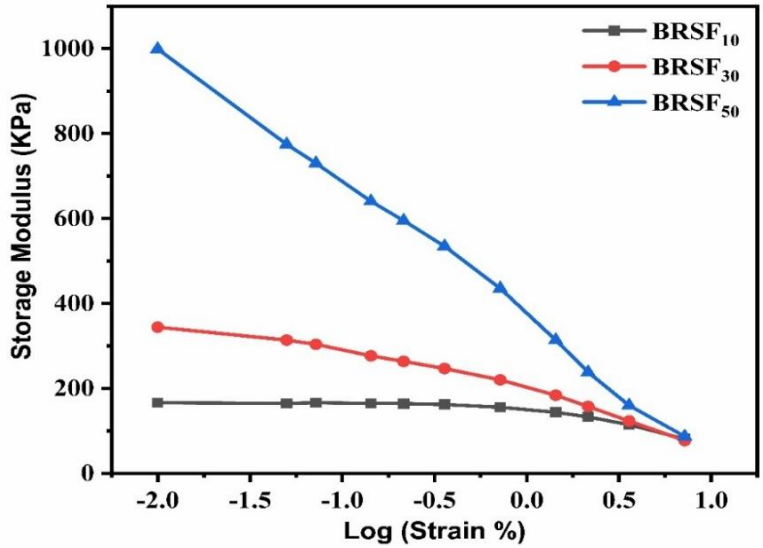

Figure 6. *Payne effect of the fabricated composite material with different fiber loadings.*

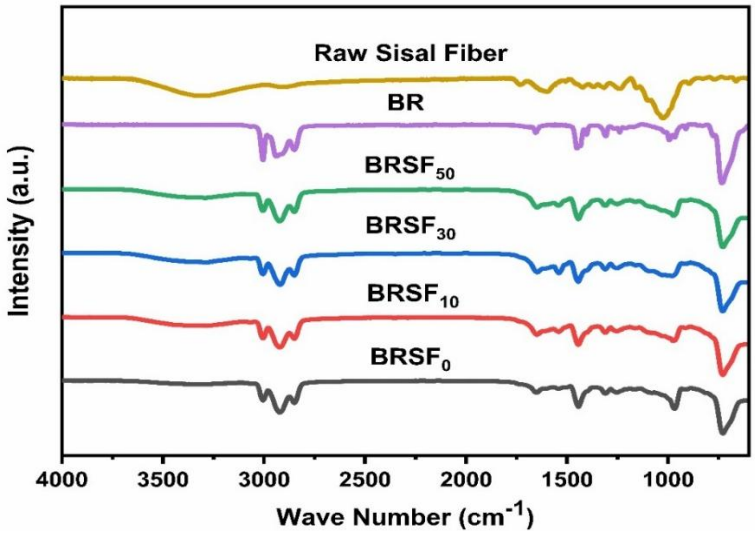

Figure 7. *FT-IR spectrum of the raw sisal fiber and fabricated composite material of different fiber loadings.*

result from the presence of hemicellulose, cellulose, and lignin ingredients. The chemical composition of BR and sisal fiber, and their interactions in the composites, was investigated using FTIR, as seen in Figure 7.

The stretching vibrations of hydroxyl (-OH) groups found in cellulose, hemicellulose, and lignin of the sisal fiber are represented by peaks in the infrared spectrum at 3410 cm^{-1} for the raw fiber and a bit lower for composites (3395 cm^{-1} for $BRSF_{10}$, 3385 cm^{-1} for $BRSF_{30}$, and 3390 cm^{-1} for $BRSF_{50,}$ respectively).[14,29] As fiber loading increased from 10 to 50 phr in the composites, there may be more physical interactions at the interface, particularly weak van der Waals forces, until the optimum fiber loading is reached; hence, a shift to lower wavenumbers was observed in Figure 7. More occurrences of these physical interactions can be observed from the increase in the overall interfacial area. While weak van der Waals forces account for the spectroscopic shift, they also promote mechanical interlocking by ensuring contact between the rubber matrix and the fiber's rough surface.[30,31] It indicates that hydroxyl groups on the fiber surface interact weakly with polymer chains, while significant hydrogen bonding is absent due to the polarity difference between the fiber and the rubber matrix. A shift toward lower wavenumbers may signify improved interactions between the fiber and BR matrix in the composites[6], as also evident in the mechanical behavior study in Figure 5. The peaks seen at 2918 and 2848 cm^{-1} correspond to the C-H stretching vibrations of -CH and -CH_2 groups in cellulose and hemicellulose.[32] The peaks seen at 1730 cm^{-1} are caused by stretching vibrations that are produced by the ester group in hemicellulose or the carbonyl group (-C = O) in the carboxylic acid of lignin. The minor peak at 1504 cm^{-1} corresponds to the C = C stretching of the aromatic ring in lignin, while the peak at 1592 cm^{-1} may be attributed to the water within the fibers, as seen in Figure 7. The observed signal at 1425 cm^{-1} is indicative of the symmetric bending of -CH_2 in cellulose.[6] In the present study, the cis form of butadiene rubber was used as the matrix material to fabricate the composite. Two distinct peaks are evident at 2848 cm^{-1} and 2917 cm^{-1} for BR, attributed to the C–H stretching of the -CH_2 groups.[33] The C = C stretching vibration of the butadiene rubber units was observed at 1638 cm^{-1}. The distinct peak at 740 cm^{-1} indicated the cis nature of the butadiene rubber used as matrix in the present study.[34]

4.4 Surface Topography Study of the Composites

An AFM study examined the surface features of vulcanized sisal fiber-reinforced butadiene rubber. The unfilled butadiene rubber showed the highest surface roughness due to its poor dimensional stability. As a result, during the AFM scanning, the stylus found more surface bumps. This led to higher roughness in the $BRSF_0$ composite than in other composites. In contrast, all sisal fiber-reinforced

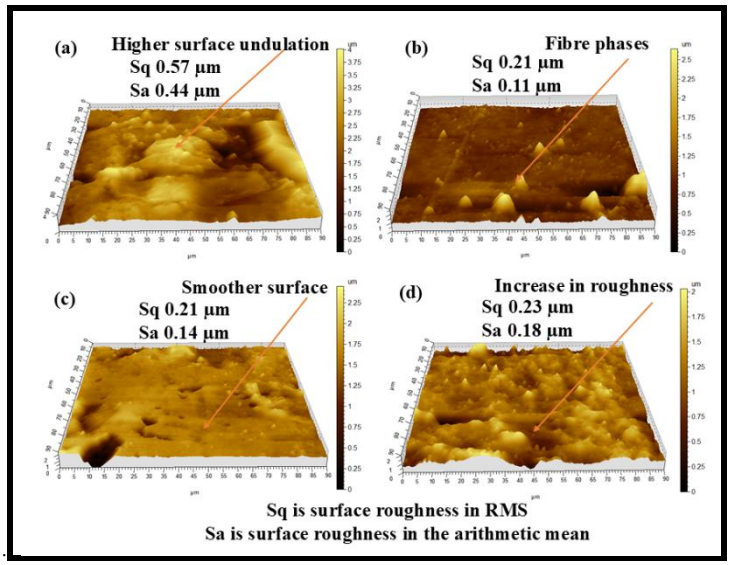

Figure 8. *AFM (3D images) study of the fabricated composites: a) BRSF$_0$, b) BRSF$_{10}$, c) BRSF$_{30}$, and d) BRSF$_{50}$.*

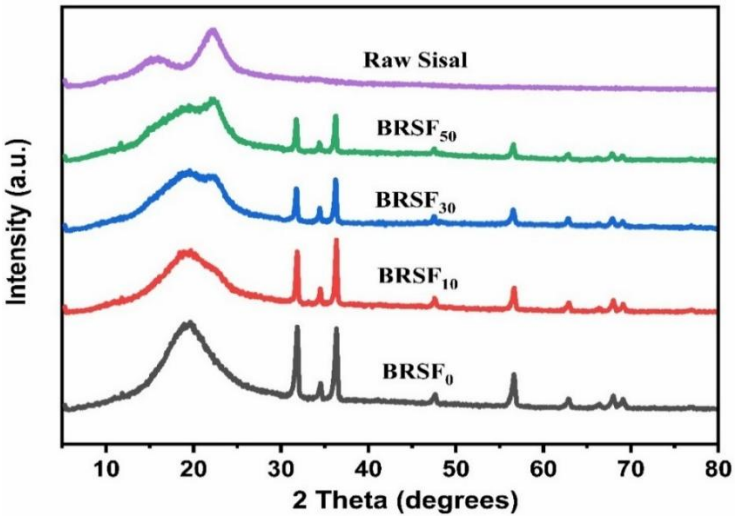

Figure 9. *The X-ray diffractograms of raw sisal fiber and its composites with different fiber loadings.*

samples had lower surface roughness than the BRSF$_0$ composite, indicating better dimensional stability. It was noticed that surface roughness consistently enhanced with an increase in fiber loading, as fibers introduced more distinct phases. The analysis showed that the fibers were nearly evenly distributed in the BRSF$_{30}$ composite. This AFM study shows that BRSF$_{30}$ exhibits greater dispersion within the rubber matrix than BRSF$_{10}$ and BRSF$_{50}$, as shown in Figure 8. This indicates that at this fiber concentration in the composite, there are significant interactions between the fiber and the rubber matrix.[35–37]

4.5 Diffraction-Based Characterization of the Composites

An essential method for examining the crystalline structure of composites made of butadiene rubber (BR) reinforced with sisal fibers is X-ray diffraction studies. This study employed high resolution x-ray diffractometer to distinguish between the crystalline regions of cellulose in sisal fiber and the amorphous phase of the BR matrix. As the fiber content in the composites escalates from BRSF$_{10}$ to BRSF$_{50}$, the region beneath each diffractogram in a pattern correspondingly increases as observed in Figure 9, indicating the amount of the crystalline phase present. The crystallinity of the composite rises from BRSF$_{10}$ to BRSF$_{50}$ with higher fiber content, as seen in Figure 9. Sisal fiber, being a lignocellulosic substance, displays distinct diffraction peaks associated with cellulose. The results exhibited two distinct peaks at 2θ values of 15.60° and 22.40° corresponding to the (101) and (002) crystallographic planes, respectively. The most pronounced peak corresponds to the (002) lattice plane of crystalline cellulose.[38] As fiber loading increases in BRSF$_{10}$ to BRSF$_{30}$ to BRSF$_{50}$, the intensity of the peak at 2θ value 22.40° with (002) crystallographic plane gradually increases, as observed in Figure 9. According to Koley and her associates, the crystalline cellulose phase of sisal fiber is the source of these diffraction patterns.[39] Using Equations (S4 and S5) in the supporting information, a notable increase in crystallinity from 36.79% to 56.69% is observed as the sisal fiber content increases from 10 phr to 50 phr in the fabricated composites. The composite's crystallinity increased linearly with fiber content, measuring 36.79% at 10 phr, 45.12% at 30 phr, and 56.69% at 50 phr.

4.6 Thermogravimetric Performance of the Sisal Fiber BR Composites

Using thermogravimetric analysis (TGA), this study explores the impact of sisal fiber on the thermal stability of BR-based composites. Important conclusions indicate variations in weight loss, residuals post-heat exposure, and degradation temperatures. The thermal degradation process of natural fiber composites, which include lignocellulosic fibers and a polymer matrix, is influenced by the specific types of matrices and reinforcements used. The main components of natural fibers, which are cellulose, hemicellulose, and lignin, decompose at distinct temperatures. The weight loss during thermal degradation occurs in three phases, namely initially moisture

Table 8. *The study of the crosslink densities of fabricated sisal fiber BR composites*

Composites	Crosslink density (mol/cm^3 × 10^{-4})
Pristine Compound (BRSF$_0$)	1.52±0.20^d
BRSF$_{10}$	1.74±0.10^c
BRSF$_{30}$	2.54±0.30^a
BRSF$_{50}$	2.15±0.10^b

All the data are represented in mean ± standard deviation. The different letters in the same column represent significant differences using Tukey's test ($p < 0.05$).

extraction, subsequent degradation of the fiber reinforcement, and final depolymerization of the matrix. Each of these phases is influenced by the fiber and matrix thermal properties and their interactions. In the TGA analysis, an initial weight loss of approximately 2% below 100 °C is observed, with the initial degradation phase occurring between 40 °C and 230 °C, mainly due to the elimination of waxy components and moisture from the sisal fibers, resulting in an approximate 3% weight loss during this interval.[40]

The second stage of sisal fiber degradation occurs between 231 and 340 °C, resulting in an 70% weight reduction, primarily due to the breakdown of hemicellulose and alpha-cellulose. Specifically, this stage shows weight reductions of 40% at 231–290 °C and 30% at 290–340 °C. The final degradation phase, occurring from 340 to 550 °C, results in a further 3.5% weight reduction and corresponds to the decomposition of lignin and other non-cellulosic components, culminating in char formation.[41] The initial decomposition temperature (IDT) for sisal fiber is about 231 °C, marking the onset of rapid deterioration, while the final decomposition temperature (FDT) is around 340 °C, indicating complete deterioration [6] as seen in Figure 10. The TGA profile of the composites is of identical nature to that of sisal fiber but shows a higher IDT, suggesting enhanced thermal stability due to the BR matrix, which protects the fiber. Furthermore, the composites' FDT is higher than that of sisal fiber, demonstrating that they are more thermally stable and take longer to fully degrade than raw sisal fiber.

Composites with a BR matrix exhibit superior thermal stability compared to their fiber counterparts, as evidenced by higher IDT and FDT values in Figure 10. The Pristine Compound with no fiber exhibits an FDT of 518 °C and an IDT of around 395 °C, representing the complete and the onset of degradation, respectively. The degradation temperatures may vary across composites with different fiber loadings; notably, the BRSF$_{10}$ composite begins to degrade at about 230 °C, whereas the BRSF$_{30}$ composite reaches a higher FDT of 535 °C, as observed in Figure 10. In contrast, the BRSF$_{50}$ composite has premature degradation due to fiber agglomeration, inadequate contact, and poor dispersion. Enhanced mechanical interlocking and optimum interaction between sisal fiber and BR in the BRSF$_{30}$ improve stress transmission and thermal stability of the composite, thereby reducing the formation of weak zones, which are more susceptible to early degradation.[42, 14]

4.7 Swelling Behavior of Sisal Fiber BR Composites

This study investigates the swelling behavior of fiber-reinforced composites, particularly sisal fiber BR composites, and their interactions with solvents, as illustrated in Table 8. This investigation reveals insights into the composites' internal structure and interfacial interactions inside the vulcanized network. Crosslink density, defined as the number of crosslinks in the BR matrix per unit volume, is significantly influenced by chemical sulfur bridges and fiber interactions. The findings of the study demonstrate a non-linear relationship between crosslink density and fiber-loaded composites, and it was carefully observed that all fiber composites showed greater crosslink density than BRSF$_0$. The presence of sisal fibers obstructs solvent flow and the expansion of rubber, hence the unbound rubber percentage decreases in the material.[43] It was observed that the crosslink densities of the BRSF$_0$ and the BRSF$_{10}$ phr fiber-loaded composite are nearly close to each other, while the BRSF$_{30}$ and BRSF$_{50}$ show elevated crosslink densities. The BRSF$_{30}$ composite notably has a higher crosslink density (Figure 11, Table 8), attributed to greater surface area and enhanced rubber-fiber interaction, aided by hydroxyl groups in the fiber and ZnO addition. Conversely, BRSF$_{50}$ exhibits a significant decline in crosslink density due to fiber agglomeration, as also evident from the morphology study in section 4.1 and Figure 4(c) of the manuscript, resulting in weakening of the BR-sisal fiber interactions,[14] correlating with decreased tensile strength as illustrated in section 4.1 and Figure 5.

4.8 Fiber Breakdown Analysis or the Aspect Ratio Study of the Composites

The assessment of fiber aspect ratio is an important feature, particularly for natural fibers used as reinforcement in composites. Natural fiber bundles can split as well as simultaneously break during compounding, thereby increasing their aspect ratio, according to research by Sabbagh and his co-workers,[44] as well as by Katharina and her colleagues.[45] Glass fibers, on the other hand, typically shorten without losing thickness, which lowers their aspect ratio. As illustrated in section 4.1 and Figure 5, splitting the fibers increases their surface area, thereby enhancing fiber integration in the rubber matrix and influencing the mechanical characteristics of the composites.

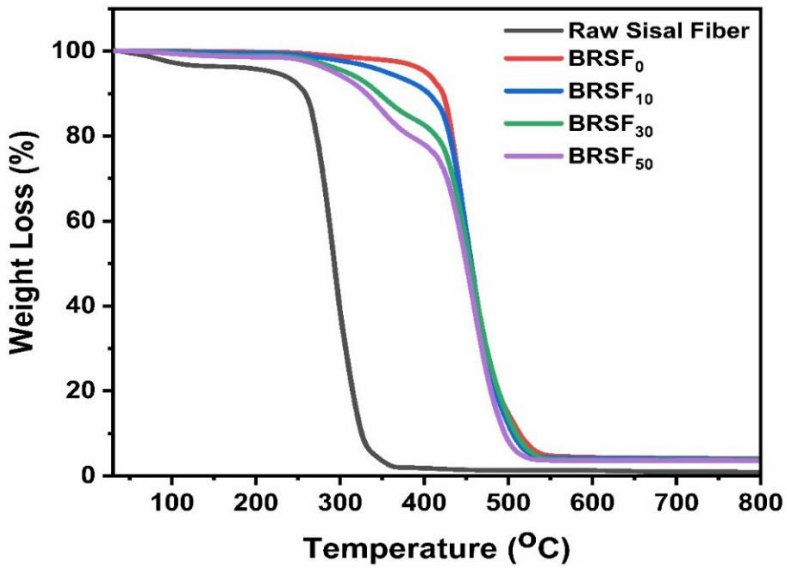

Figure 10. *Comparative study of thermogravimetric analysis plots for sisal fiber-reinforced BR composites.*

Table 9. *The study of the composite's aspect ratio with different fiber loadings.*

Different fiber-loaded composites	Length of fiber (mm)	Diameter of fiber (mm)	Aspect Ratio
Raw Sisal Fiber	4.66±0.24^{a}	0.27±0.04^{a}	17.26±0.06^{a}
BRSF$_{10}$	2.87±0.04^{b}	0.19±0.02^{a}	15.10±0.03^{b}
BRSF$_{30}$	2.71±0.01^{bc}	0.17±0.03^{ab}	15.94±0.02^{b}
BRSF$_{50}$	2.35±0.03^{c}	0.15±0.02^{b}	15.66±0.01^{b}

All the data are represented in mean ± standard deviation. The different letters in the same column represent significant differences using Tukey's test (p <0.05).

Table 9 shows the measured lengths and widths of sisal fibers. Sisal fiber's dimensions are greatly changed by compounding. It has been carefully observed that when fibers simply break (length reduction) instead of splitting (breadth or diameter preservation), the aspect ratio drops. Glass and carbon fibers exhibit this pattern. However, the aspect ratio might not decrease during processing steps for natural fibers like sisal, as fiber bundles fracture and break. The study in this manuscript shows that after compounding, the sisal fiber aspect ratio changed significantly. Furthermore, the incidence of fiber fracture increases with increasing matrix fiber concentration.[45] Compared to greater fiber loadings, reduced fiber content in the BRSF$_{10}$ composite led to less fiber breakage. Sisal fibers tend to break up into smaller segments due to the higher shearing forces during compounding, which also lowers the bundle diameter. In BRSF$_{30}$ composites, an ideal aspect ratio was achieved, associated with improved mechanical properties (Figure 5) and efficient fiber dispersion, ensuring sufficient contact with the rubber matrix. After this point, additional increases in fiber loading in the composite caused the aspect ratio to drop as the fibers fractured and agglomerated, impairing alignment and stress-bearing capacity.[46] Table 9 provides a clear illustration of the variation in the aspect ratio of the fabricated composites.

4.9 Water Absorption Behavior Study of the Composites

Excess water absorption by cellulosic fibers is a major drawback that adversely affects the mechanical properties of composites. These fibers' hydrophilic properties, largely due to hydrogen bonds in their cell walls, allow them to absorb moisture. These hydrogen bonds break when exposed to moisture because hydroxyl groups form new bonds with water molecules, increasing water absorption. This issue can be resolved by methods like surface modification and polymer coating. However, because of their propensity to absorb moisture,

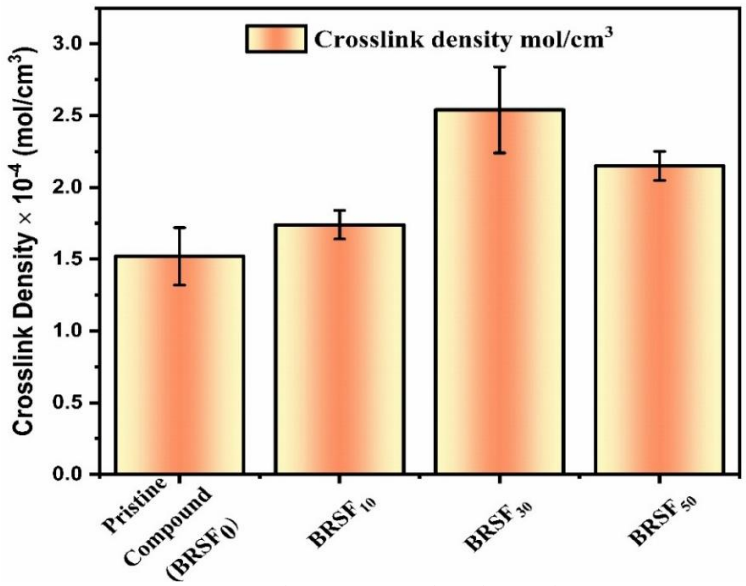

Figure 11. *Comparative study of crosslink density of sisal fiber-reinforced BR composites.*

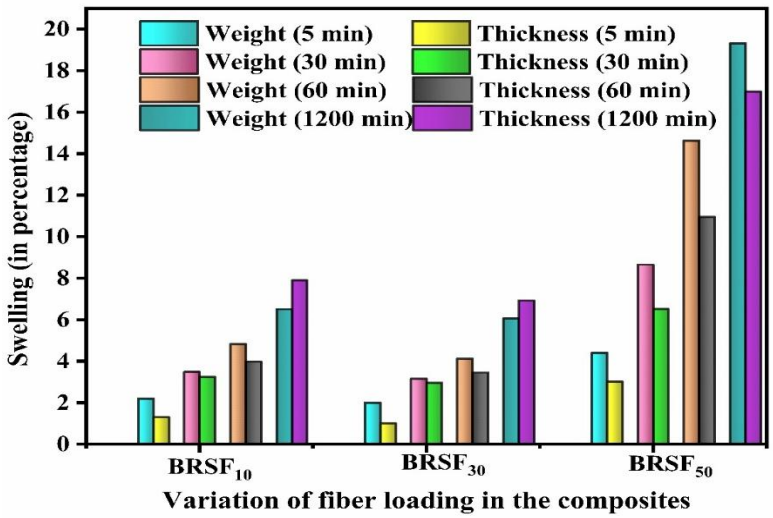

Figure 12. *Water absorption behavior of composites at different time intervals.*

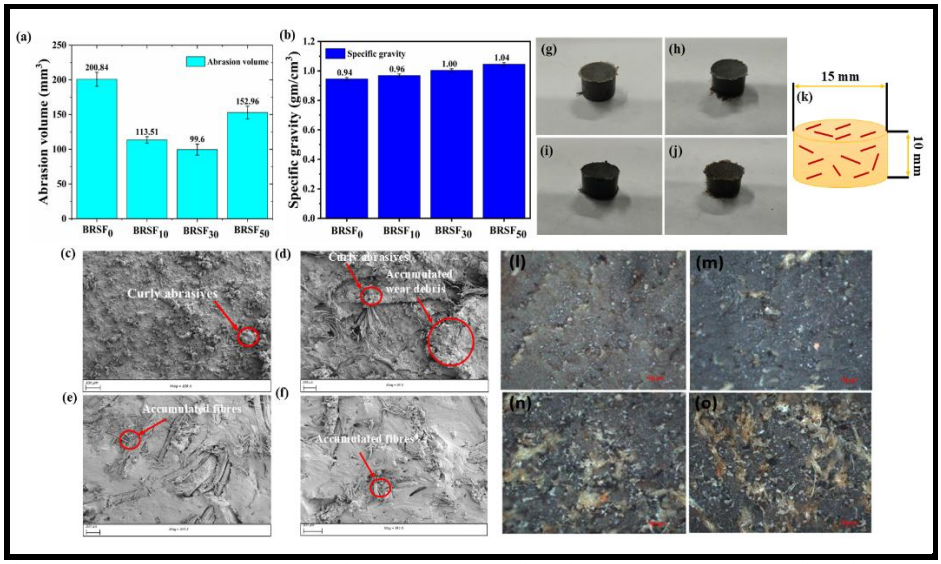

Figure 13. *Abrasion test of composites: (a) Abrasion volume, (b) Specific gravity, (c) Worn surface of pristine ($BRSF_0$), (d) Worn surface of $BRSF_{10}$, (e) Worn surface of $BRSF_{30}$, (f) Worn surface of $BRSF_{50}$, Visual images of abarsion sample buttons for (g) Pristine ($BRSF_0$), (h) $BRSF_{10}$, (i) $BRSF_{30}$, (j) $BRSF_{50}$, (k) Button dimension, Optical microscopy images of the worn surface of the composites (l) $BRSF_0$, (m) $BRSF_{10}$, (n) $BRSF_{30}$, and (o) $BRSF_{50}$.*

natural fiber polymer composites are typically considered inappropriate for outdoor applications or settings with heavy water exposure. These composites show significant moisture absorption in humid environments or when immersed, which may have an impact on their functionality. Interfacial bonding is disrupted by the plasticizing effect of absorbed water, which results in inadequate stress transfer and deterioration of mechanical properties.[47] The hydrophilic nature of these fibers is closely associated with the hydroxyl groups present in cellulose, hemicellulose, and lignin, which bind water molecules through hydrogen bonds. Variations in the chemical composition of different cellulosic fibers result in differing water-absorption capacities, with hemicellulose as the primary contributor, followed by amorphous cellulose, lignin, and crystalline cellulose. Additionally, other factors influencing water absorption include fiber properties, surface area exposure to water, reinforcement architecture, degree of crystallinity, and interfacial bonding between the cellulosic fibers and polymers.

After thirty and sixty minutes, all samples exhibited swelling percentages below 8 %. However, after 20 hours, the $BRSF_{50}$ composite showed a notable increase in water absorption of approximately 19.32%, with a viscous, white appearance. Importantly, after eight days, no samples showed significant weight changes. Sahu and his colleagues reported that composites with higher fiber content exhibited greater water absorption, resulting in swelling.[48] This absorption tendency increased with the fiber loading, except for the $BRSF_{30}$ composite. Higher natural fiber loading increases the number of hydroxyl groups and micro-voids, thereby enhancing moisture absorption due to their hydrophilicity.[49] The optimal interaction at the interface in $BRSF_{30}$ reduces voids and microcracks that might allow moisture penetration, as demonstrated in the SEM micrograph in Figure 4(b). Additionally, in $BRSF_{30}$, efficient crosslinking forms a 3D network within the rubber matrix, reducing polymer chain mobility and thus limiting moisture ingress to 6.05%. Crosslink density can be correlated with the composites' water absorption properties: increased crosslinking leads to reduced water absorption, as observed in Figures 11 and 12.

4.10 Abrasion Study of the Composites

The abrasion volume gradually decreased with the incorporation of 10 phr and 30 phr of sisal fiber, but it increased again at 50 phr, as observed in Figure 13(a). Specifically, when incorporating 10 phr, 30 phr, and 50 phr of fiber, the abrasion volume loss was reduced by approximately 43.48%, 50.41%, and 23.84%, in comparison to the pristine compound, as shown in Table 10. This explains a considerable improvement in wear resistance with the addition of sisal fiber. On incorporation of 10 phr, 30 phr, and 50 phr sisal fiber, the abrasion resistance increased by about 77%, 102%, and 31%, respectively. The specific gravity increased gradually with increasing sisal fiber content, as observed in Figure 13(b). The curly abrasive shows higher wear volume than the grainy abrasive, as observed in SEM micrographs in Figure 13(c-f). Figure 13(c) shows that a significant number of curly abrasives were present, indicating a higher abrasion volume in the pristine compound. As the sisal fiber content increased, the abrasive effect of the sisal fiber gradually decreased, as observed in Figures 13(d-f). The worn surface of $BRSF_{10}$ displayed a small amount of curly abrasives and a considerable amount of accumulated wear debris as observed in Figure 13(d). In contrast, very negligible curly abrasives were observed on the worn surface of $BRSF_{30}$, indicating its superior wear resistance compared to the other composites.[50] Although there was no curly wear debris present on the worn surface of $BRSF_{50}$, many accumulated fibers were lost due to lower rubber-to-fiber interaction[51] as seen in Figure 13(f), which actually increased the wear volume compared to $BRSF_{10}$ and $BRSF_{30}$. Optical microscopy images of the worn surfaces of the button-shaped composites are shown in Figure 13 (l-o). Materials with stable, consistent wear tracks tend to exhibit reduced wear loss, as this is associated with a more controlled removal process that minimizes surface damage, as observed for the 30 phr fiber-loaded composite in Figure 13(n). In contrast, uneven and fragmented wear patterns result in greater wear loss due to increased crack propagation and abrasive detachment, leading to significant material degradation as observed for the pristine compound in Figure 13(l). The continuous grooves are formed in the wear direction, and fibers are oriented in that direction, providing a clear picture of the wear tracks observed in the optical microscopy images in Figure 13(l-o).

Table 10. *The study of the abrasion volume of the composites.*

Sample ID	Abrasion volume (mm^3)
$BRSF_0$	200.84 ± 10.04^a
$BRSF_{10}$	113.51 ± 4.54^c
$BRSF_{30}$	99.60 ± 7.96^d
$BRSF_{50}$	152.96 ± 9.17^b

All the data are represented in mean ± standard deviation. The different letters in the same column represent significant differences using Tukey's test ($p < 0.05$).

4.11 Soil Burial and Environmental Exposure Studies of the Composites

The soil biodegradability test of the fabricated composite has been assessed and compared with that of the pristine compound. The present study investigated the stability of developed composites

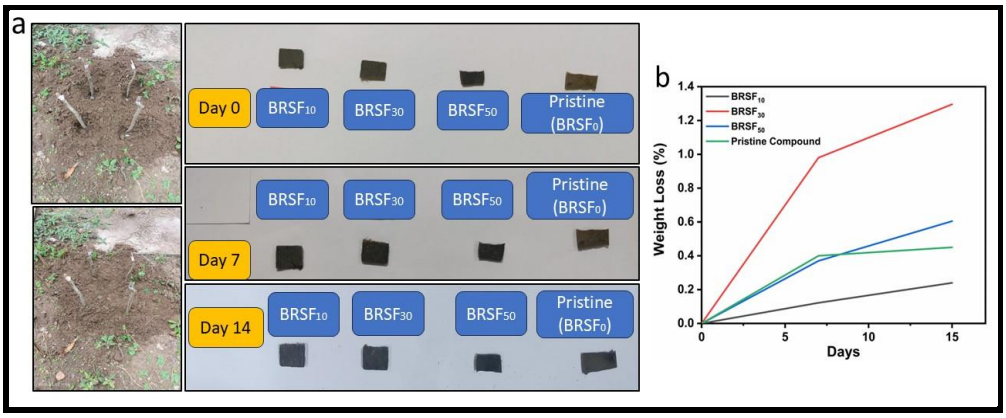

Figure 14. *Soil burial studies performed on the fabricated composites (a) visual appearance and color (b) weight loss for 15 days.*

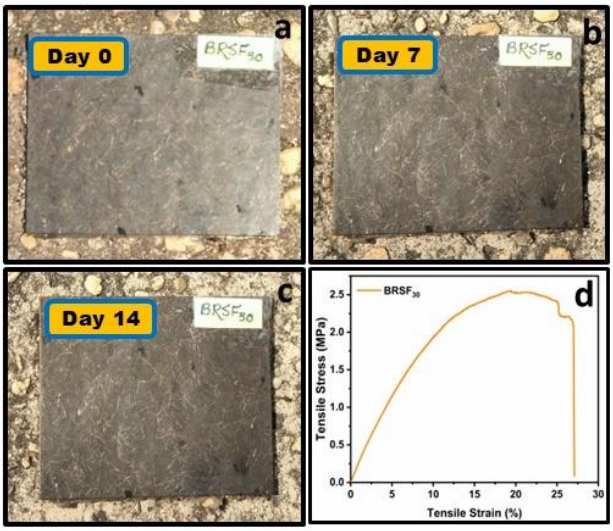

Figure 15. *Environmental exposure (open air) studies performed on the BRSF30 composite (a-c) visual appearance and color (d) change in tensile strength after 2 weeks.*

under specific conditions, including soil burial at pH 5.50 and a moisture content of 45% by weight. The composites were visually examined and showed no significant color change during the study, as observed in Figure 14(a). The initial weight of the composites is 0.16 gm ($BRSF_{10}$), 0.16 gm ($BRSF_{30}$), 0.13 gm ($BRSF_{50}$), and 0.17 gm ($BRSF_0$), respectively. It is clearly evident from Figure 14(b) that from day 0 to day 15, the pristine compound incurs an insignificant weight loss of 0.05 percent. In contrast, the composites incorporated with sisal fiber showed noticeable weight losses of 0.11, 0.31, and 0.28 percent, respectively. This is certainly due to the biodegradable nature of sisal fiber, contributing to the degradation of the composites.[52]

Moreover, among the composites with different fiber loadings, it has been observed that $BRSF_{30}$ and $BRSF_{50}$ exhibit weight loss percentages of 0.31% and 0.28%, respectively, on day 15. Whereas $BRSF_{10}$ showed a 0.11% decrease in weight. According to the literature, the higher the sisal fiber concentration in the composites, the greater the likelihood of degradation.[53] However, a slight deviation in our study showed that the weight-loss percentage for $BRSF_{30}$ was greater than that for $BRSF_{50}$, likely because the initial weight of $BRSF_{50}$ was much lower than that of $BRSF_{30}$.

A durability assessment of the $BRSF_{30}$ composite was conducted by continuous exposure to open-air conditions for 2 weeks, followed by tensile testing in accordance with ASTM D3039.[54] Moisture absorption plays a critical role in determining the shelf life of natural fiber-reinforced composites (NFRCs), as natural fibers are hygroscopic and can absorb moisture, leading to fiber expansion and weakening of the fiber-polymer matrix bond, as discussed already in section 4.9 of the manuscript. Environmental conditions, including temperature fluctuations, significantly affect NFRC's durability; high temperatures may accelerate degradation, while extreme cold can cause brittleness, as reported by Arunprasth and his colleagues.[54] As per a study by Moll and his colleagues, UV radiation from the sun also poses a risk to the composite's surface, leading to color fading and loss of structural integrity.[55] Proper storage conditions, such as climate-controlled environments, are essential for preserving material quality, whereas exposure to humidity and sunlight can lead to performance deterioration, as reported by Paudel and his co-workers.[56] A study on jute-epoxy composites under high-humidity conditions found a 15% increase in water absorption and a 20% reduction in tensile strength after six months, as noted by Arunprasth and colleagues,[54] In experiments with UV light on hemp-polyester composites, a 30% strength loss occurred after 1000 hours of exposure, suggesting a shelf life of about one year. Conversely, kenaf-polypropylene composites showed a more moderate 15% decrease in strength after six months of natural weathering, while UV stabilizers provided some mitigation, as reported by Arif and his co-workers.[57] The present study observed minimal color change, as observed in Figure 15(a-c), and a marginal 0.12% weight gain due to moisture absorption after 2 weeks in the $BRSF_{30}$ composite, indicating the composite's stability. Moreover, tensile-strength evaluation indicated tensile strength retention of 75.66% in the $BRSF_{30}$ composite assessed after 2 weeks, as illustrated in Figure 15 (d).

5. Conclusions and Future Scope of Work

In conclusion, the study presents a novel composite material made from BR (butadiene rubber) and sisal fiber, specifically designed for indoor mat applications. The composites were prepared

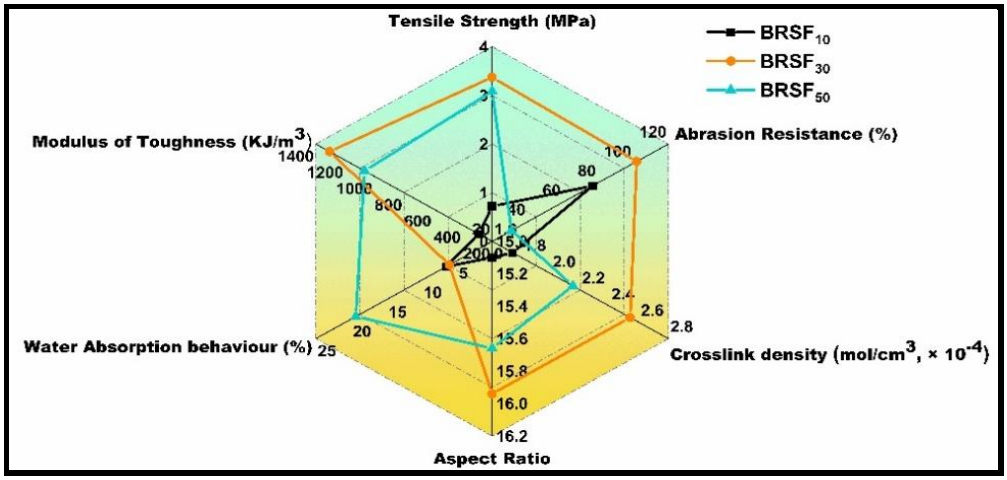

Figure 16. *Radar plot showing the performance of all the composites.*

using a Haake Rheomix® laboratory internal mixer, with various sisal fiber loadings being tested. The multiscale characterization of the fabricated composite material in this manuscript includes morphology studies, crystallinity, tensile performance, thermal analysis, aspect ratio, crosslink density, soil burial tests, and abrasion studies. The chopped fiber length used in this study was 4-5.50 mm, which was blended non uniformly with the BR matrix. Morphological analysis revealed that mechanical stresses and breakage during mixing reduced the average length and diameter of the sisal fibers from their initial dimensions used in this study. The micrographs showed that $BRSF_{30}$ has very few air-trapped holes and a relatively uniform fiber distribution, compared to other fabricated composites. The topographical study provides information that the surface of $BRSF_{30}$ was uniform, with strong fiber-rubber interaction. The optimum tensile strength of 3.37 ± 0.51 MPa was achieved for $BRSF_{30}$, due to uniform fiber distribution and strong fiber-rubber interaction. Hence, the maximum stress can be effectively transferred from the matrix to the fiber at this particular fiber concentration in the composite. In contrast, in $BRSF_{50}$, fiber agglomerates and thus poor fiber-matrix interaction prevent effective transfer of stress from the matrix to the fibers, resulting in a decrease in tensile strength compared to $BRSF_{30}$. Diffraction studies clearly showed the highest crystallinity for $BRSF_{50}$, due to its higher fiber content in the composites. The $BRSF_{50}$ had a maximum water absorption rate of 19.32 percent. Additionally, the $BRSF_{30}$ has an optimum aspect ratio and crosslink density of 15.94 ± 0.02 and 2.54 ± 0.30 mol/cm^3 × 10^{-4}, respectively. In the abrasion study with the fabricated composites, it was observed that for $BRSF_{30}$, the abrasion volume loss decreased by 50.41 percent, and the abrasion resistance increased by 102 percent compared to $BRSF_0$. The results of this study indicate that sisal fiber, which is economical and eco-friendly, improved the properties of the BR composites, including interaction, abrasion resistance, tensile strength, thermal behavior, crosslink density, and aspect ratio. The summary of the whole study is presented in a radar plot in Figure 16, which suggests that lightweight $BRSF_Y$ composites may have the potential to serve as a novel platform for commodity rubber goods applications.

The present work highlights the potential of sisal, an agricultural waste, as a replacement for carbon-intensive synthetic fillers in the elastomer industry, contributing to global "Green Chemistry" initiatives. Future research avenues include investigating silane coupling agents and alkali pretreatments to enhance interfacial adhesion and mitigate leaching observed during water immersion. Further exploration of bio-derived coupling agents and green surface treatments, such as cold plasma or enzymatic modification, may improve sisal's hydrophobicity. Additionally, hybridizing sisal fibers with nanofillers like carbon nanotubes or graphene could balance stiffness and flexibility. Extending soil burial and UV-aging studies to 6–12 months will yield insights into the lifecycle and degradability of the bio-composites. A more detailed study of the Payne Effect and the temperature-dependent storage modulus will enhance understanding of the damping properties essential for vibration-isolation applications. Conducting a formal life cycle assessment (LCA) could quantify the carbon footprint reduction achieved by transitioning from carbon-black-filled to sisal-filled rubber composites. This research establishes sisal as a viable, sustainable reinforcement for butadiene rubber matrices, marking a shift toward bio-based engineering materials. It reveals that while high-loading composites ($BRSF_{50}$) demonstrate superior hardness and rigidity, the $BRSF_{30}$ variant strikes a better balance in chemical and physical properties. Transitioning to natural fillers addresses environmental concerns and raw material cost fluctuations, prompting future research to optimize the fiber-matrix interface through advanced chemical treatments to increase application potential in humid or dynamic underwater environments.

Supporting Information

The supplementary information for this article is available in the Supporting Information at https://insuf.org/icms/icms.2026.03055SI.pdf

Author Contribution Declaration

Souvik Das: Writing original draft, Testing, and Characterizations. **Himon Sen:** Writing, Testing, and Characterizations, **Payel Dasgupta:** Testing and Characterization. **Vivek Kumar Yadav:** Testing and Characterization. **Narayan Ch. Das:** Supervision, Writing - review & editing. **Debasish Das:** Supervision, Writing - review & editing.

Attention: The authors have no financial conflicts of interest to disclose.

Author Information

Corresponding Authors
Narayan Ch. Das- Rubber Technology Centre, Indian Institute of Technology Kharagpur, Kharagpur, West Bengal, 721302, India.
Email: ncdas@rtc.iitkgp.ac.in
https://orcid.org/0000-0002-5945-7457
Debasish Das- Department of Jute and Fiber Technology, University of Calcutta, Kolkata, 700019, India.
Email: ddjf@caluniv.ac.in
https://orcid.org/0009-0002-3795-8362

Authors
Souvik Das- Department of Jute and Fiber Technology, University of Calcutta, Kolkata, 700019, India.
https://orcid.org/0009-0008-0265-5760
Himon Sen- Rubber Technology Centre, Indian Institute of Technology Kharagpur, Kharagpur, West Bengal, 721302, India.
https://orcid.org/0009-0005-9164-8180

Payel Dasgupta- Agricultural and Food Engineering Department, Indian Institute of Technology Kharagpur, Kharagpur, West Bengal, 721302, India.
https://orcid.org/0009-0001-2510-061X
Vivek K. Yadav- Rubber Technology Centre, Indian Institute of Technology Kharagpur, Kharagpur, West Bengal, 721302, India.
https://orcid.org/0009-0006-9254-0611

Funding Sources

No funding source.

Data Availability Declaration

The authors declare that the data supporting the findings are available within the article.

Conflict of Interest Statement

The authors declare that they have no conflict of interest in this research article.

Acknowledgements

The authors appreciate the cooperation of the Rubber Technology Center at the Indian Institute of Technology (IIT), Kharagpur (India), 721302. The author acknowledges the Department of Jute and Fiber Technology, University of Calcutta, Kolkata, India, 700019, for this work.

References

1. F. M. Khan, A. H. Shah, S. Wang, S. Mehmood, J. Wang, W. Liu, X. Xu. A Comprehensive Review on Epoxy Biocomposites Based on Natural Fibers and Bio-fillers: Challenges, Recent Developments and Applications. *Advanced Fiber Materials.* **2022**, *4*, 683. https://doi.org/10.1007/s42765-022-00143-w
2. M. R. M. Asyraf, T. Khan, A. Syamsir, A. B. M. Supian. Synthetic and Natural Fiber-Reinforced Polymer Matrix Composites for Advanced Applications. *Materials*. **2022**, *15*, 6030. https://doi.org/10.3390/ma15176030
3. J. Hu, S. Zhang, J. Lin, Y. Yu, W. Yu, Y. Huang. Towards Sustainable High-Performance Materials: Tailoring the Mechanical Properties of Bamboo-Based Fiber Composites through Controlled Processing. *Chemical Engineering Journal*. **2025**, *512*, 162331. https://doi.org/10.1016/j.cej.2025.162331
4. U. V. Akhil, N. Radhika, B. Saleh, S. Aravind Krishna, N. Noble, L. Rajeshkumar. A comprehensive review on plant-based natural fiber reinforced polymer composites: Fabrication, properties, and applications. *Polym. Compos.* **2023**, *44*, 2598. https://doi.org/10.1002/pc.27274
5. S. Sayam. Natural fibers in sustainable materials: extraction technologies, fiber modification, and performance–sustainability relationships. *RSC Adv.* **2026**, *16*, 10495. https://doi.org/10.1039/d5ra09029f
6. S. Das, J. Nayak, P. Das, N. C. Das, D. Das. An investigation on sisal fiber reinforced nitrile butadiene rubber composites. *Journal of Polymer Research*. **2025**, *32*, 1. https://doi.org/10.1007/s10965-025-04631-6
7. B. Hajare, R.K. Shuib. A comprehensive review on rubber-based adhesives. *J. Adhes. Sci. Technol.* **2025**, *39*, 1133. https://doi.org/10.1080/01694243.2024.2447456
8. K. K. Khoaele, I. J. Mphahlele, O. J. Gbadeyan, B. Sithole, V. Chunilall. Current Approaches on Natural Fiber Reinforcement Surface Treatment for Construction Material Application. *Int. J. Polym. Sci.* **2024**, *2024*, 1. https://doi.org/10.1155/2024/1387468
9. D. Shelly, V. Singhal, S. Jaidka, M. D. Banea, S.Y. Lee, S.J. Park. Mechanical performance of bio-based fiber reinforced polymer composites: A review. *Polym. Compos.* **2025**, *46*, S9. https://doi.org/10.1002/pc.30000
10. I. Goda, E. Padayodi, R. N. Raoelison. Enhancing fiber/matrix interface adhesion in polymer composites: Mechanical characterization methods and progress in interface modification. *J. Compos. Mater*. **2024**, *58*, 3077. https://doi.org/10.1177/00219983241283958
11. Y. A. El-Shekeil, Faris M. AL-Oqla, H. A. Refaey, S. Bendoukha, N. Barhoumi. Investigating the mechanical performance and characteristics of nitrile butadiene rubber date palm fiber reinforced composites for sustainable bio-based materials. *Journal of Materials Research and Technology*. **2024**, *29*, 101. https://doi.org/10.1016/j.jmrt.2024.01.092
12. K. Venkatesan, G. B. Bhaskar. Evaluation and Comparison of Mechanical Properties of Natural Fiber Abaca-sisal Composite. *Fibers and Polymers*. **2020**, *21*, 1523. https://doi.org/10.1007/s12221-020-9532-5
13. S. M. R. Paran, G. Naderi, S. Shokoohi, J. Ebadati, C. Dubois. Mechanical and Thermal Properties of Green Thermoplastic Elastomer Vulcanizate Nanocomposites Based on Poly (vinyl chloride) and Nitrile Butadiene Rubber Containing Organoclay and Rice Straw Natural Fibers. *J Polym. Environ.* **2019**, *27*, 2017. https://doi.org/10.1007/s10924-019-01491-2
14. S. Das, P. Das, N.Ch. Das, D. Das. An investigation on sisal fiber reinforced carboxylate nitrile butadiene rubber composites. *Next Research*. **2025**, *2*, 100450. https://doi.org/10.1016/j.nexres.2025.100450
15. C. Ajay, S. Das Gupta, R. Mukhopadhyay, D. Chattopadhyay, M. Das. Exploring crosslink density in rubber vulcanisates - a comprehensive analysis using a dynamic mechanical analyser and an insight into mechanical properties. *Journal of Rubber Research*. **2025**, *28*, 305. https://doi.org/10.1007/s42464-025-00305-6
16. M. Andideh, M. H. R. Ghoreishy. Rubber-based short fiber reinforced composites. *Rubber Technology*. **2026**, 245. https://doi.org/10.1016/B978-0-12-823826-4.00018-2
17. C. Rong-or, W. Pongputthipat, Y. Ruksakulpiwat, P. Chumsamrong. Soil burial degradation of bio-composite films from poly(lactic acid), natural rubber, and rice straw. *Polymer Bulletin*. **2024**, *81*, 10729. https://doi.org/10.1007/s00289-024-05229-6
18. C. Tóth, K. Molnár, Á. D. Virág. Short fiber reinforcement in material extrusion 3D printing: A meta-analysis review with insights into sustainable alternatives. *Polym. Compos.* **2025**, *46*, S9. https://doi.org/10.1002/pc.29850
19. L. Xu, L. Fang, Z. Zheng, J. Zhou, X. Zheng, Q. Gao, Z. Xu, H. Lian, C. Xu. Advances in investigating the interfacial compatibility of treated bamboo fibers with non-polar polymer matrices. *Compos. Interfaces*. **2025**, *33*, 235. https://doi.org/10.1080/09276440.2025.2518795
20. M. D. Stelescu, E. Manaila, G. Craciun, C. Chirila. Development and characterization of polymer eco-composites based on natural rubber reinforced with natural fibers. *Materials*. **2017**, *10*, 1. https://doi.org/10.3390/ma10070787
21. D. Wong, G. Fabito, S. Debnath, M. Anwar, I. J. Davies. A critical review: Recent developments of natural fiber/rubber reinforced polymer composites. *Cleaner Materials*. **2024**, *13*, 1. https://doi.org/10.1016/j.clema.2024.100261
22. S. Saravanakumar, S. Sathiyamurthy, V. Vinoth, P. Devi. Effect of Alumina on Epoxy Composites with Banana Fiber: Mechanical, Water Resistance and Degradation Property Analysis. *Fibers and Polymers*. **2024**, *25*, 275. https://doi.org/10.1007/s12221-023-00405-3
23. M. Idicula, N. R. Neelakantan, Z. Oommen, K. Joseph, S. Thomas. A study of the mechanical properties of randomly oriented short banana and sisal hybrid fiber reinforced polyester composites. *J. Appl. Polym. Sci.* **2005**, *96*, 1699. https://doi.org/10.1002/app.21636
24. J. A. K. M. Fernando, C. Yalegama, N. Fernando, U. K. Samarakoon, D. Edirisinghe, M. Sampath. Characterization of the coir fiber from different coconut varieties to enhance the performance of coir fiber-reinforced natural rubber composites. *Journal of Elastomers and Plastics*. **2025**, *57*, 475. https://doi.org/10.1177/00952443251323933
25. L. Bokobza. Elastomer Nanocomposites: Effect of Filler–Matrix and Filler–Filler Interactions. *Polymers (Basel)*. **2023**, *15*, 1. https://doi.org/10.3390/polym15132900
26. S. M. R. Paran. Nonlinear viscoelasticity and Payne effect of nanocellulose reinforced elastomer composites. *Elastomeric Nanocellulose Composites*. **2024**, 301. https://doi.org/10.1016/B978-0-443-18608-0.00006-1
27. Y. Xiao, B. Li, Y. Huang, Z. Gong, P. Diao, C. Wang, H. Bian. High-value application of kaolin by wet mixing method in low heat generation and high wear-resistant natural rubber composites. *Appl. Clay Sci.* **2024**, *261*, 1. https://doi.org/10.1016/j.clay.2024.107574
28. C. Güner, A. Manzak. Investigating the influence of alkali treated hemp fibre on the mechanical properties of diverse rubber composites. *Journal of Rubber Research*. **2025**, *28*, 159. https://doi.org/10.1007/s42464-025-00294-6
29. R. Gheribi, Y. Taleb, L. Perrin, C. Segovia, N. Brosse, S. Desobry. Development of Chitosan Green Composites Reinforced with Hemp Fibers: Study of Mechanical and Barrier Properties for Packaging Application. *Molecules*. **2023**, *28*, 1. https://doi.org/10.3390/molecules28114488

30. D. Gunwant. Moisture resistance treatments of natural fiber-reinforced composites: a review. *Compos. Interfaces*. **2024**, *31*, 979. https://doi.org/10.1080/09276440.2024.2303543
31. M. Jacob, S. Joseph, L. A. Pothan, S. Thomas. A study of advances in characterization of interfaces and fiber surfaces in lignocellulosic fiber-reinforced composites. *Compos. Interfaces*. **2005**, *12*, 95. https://doi.org/10.1163/1568554053542115
32. M. D. Stelescu, A. Airinei, A. Bargan, N. Fifere, M. Georgescu, M. Sonmez, M. Nituica, L. Alexandrescu, A. Stefan. Mechanical Properties and Equilibrium Swelling Characteristics of Some Polymer Composites Based on Ethylene Propylene Diene Terpolymer (EPDM) Reinforced with Hemp Fibers. *Materials*. **2022**, *15*, 1. https://doi.org/10.3390/ma15196838
33. S. Hait, J. L. Valentín, A. G. Jiménez, P. B. Ortega, A. K. Ghosh, K. W. Stöckelhuber, S. Wießner, G. Heinrich, A. Das. Poly(acrylonitrile-co-butadiene) as polymeric crosslinking accelerator for sulphur network formation. *Heliyon*. **2020**, *6*, 1. https://doi.org/10.1016/j.heliyon.2020.e04659
34. J. Lv, J. Feng. Forensic evaluation of 10 types of rubber popularly used with Fourier transform infrared (FTIR) spectroscopy. *International Journal of Polymer Analysis and Characterization*. **2025**, *30*, 603. https://doi.org/10.1080/1023666X.2025.2496299
35. L. Johnson. Atomic Force Microscopy (AFM) for rubber. *Rubber Chemistry and Technology*. **2008**, *81*, 359. https://doi.org/10.5254/1.3548214
36. S. S. Kumar, P. Shyamala, P. R. Pati, D. K. Mishra, V. Sharma, G. Tank, M. Kanan. Investigation and machine learning-based prediction of mechanical properties in hybrid natural fiber composites. *Sci. Rep*. **2025**, *15*, 1. https://doi.org/10.1038/s41598-025-18944-5
37. Tirupathi, J. S. Kumar, S. S. Hiremath. Investigation of Mechanical Characterisation and Thermal Performance of Hybrid Natural Fiber Composites for Automotive Applications. *Fibers and Polymers*. **2022**, *23*, 3505. https://doi.org/10.1007/s12221-022-4576-3
38. F. D. Xavier, G. S. Bezerra, S. F. M. Santos, L. S. C. Oliveira, F. L. H. Silva, A. J. O. Silva, M. M. Conceição. Evaluation of the simultaneous production of xylitol and ethanol from sisal fiber. *Biomolecules*. **2018**, *8*, 1. https://doi.org/10.3390/biom8010002
39. R. Koley, U. K. Ghorai, S. Chattopadhyay, A. K. Bhowmick. An investigation on Moringa oleifera fruit (drumstick)-derived cellulose micro and nanofiber reinforced styrene butadiene rubber composites. *Polym. Compos.* **2023**, *44*, 2778. https://doi.org/10.1002/pc.27279
40. S. Behera, R. K. Gautam, S. Mohan. The effect of eco-friendly chemical treatment on sisal fiber and its epoxy composites: thermal, mechanical, tribological and morphological properties. *Cellulose*. **2022**, *29*, 9055. https://doi.org/10.1007/s10570-022-04826-w
41. A. Veerasimman, V. Shanmugam, S. Rajendran, D. J. Johnson, A. Subbiah, J. Koilpichai, U. Marimuthu. Thermal Properties of Natural Fiber Sisal Based Hybrid Composites–A Brief Review. *Journal of Natural Fibers*. **2022**, *19*, 4696. https://doi.org/10.1080/15440478.2020.1870619
42. N. M. Nurazzi, M. R. M. Asyraf, M. Rayung, M. N. F. Norrrahim, S. S. Shazleen, M. S. A. Rani, A. R. Shafi, H. A. Aisyah, M. H. M. Radzi, F. A. Sabaruddin, R. A. Ilyas, E. S. Zainudin, K. Abdan. Thermogravimetric analysis properties of cellulosic natural fiber polymer composites: A review on influence of chemical treatments. *Polymers (Basel)*. **2021**, *13*, 1. https://doi.org/10.3390/polym13162710
43. M. Y. Mahmoud Zaghloul, M. M. Yousry Zaghloul, M. M. Yousry Zaghloul. Developments in polyester composite materials – An in-depth review on natural fibres and nano fillers. *Compos. Struct.* **2021**, *278*. https://doi.org/10.1016/j.compstruct.2021.114698
44. A. M. M. El-Sabbagh, L. Steuernagel, D. Meiners, G. Ziegmann. Effect of extruder elements on fiber dimensions and mechanical properties of bast natural fiber polypropylene composites. *J. Appl. Polym. Sci.* **2014**, *131*, 1. https://doi.org/10.1002/app.40435
45. K. Albrecht, T. Osswald, E. Baur, T. Meier, S. Wartzack, J. Müssig. Fibre length reduction in natural fibre-reinforced polymers during compounding and injection moulding—experiments versus numerical prediction of fibre breakage. *Journal of Composites Science*. **2018**, *2*, 1. https://doi.org/10.3390/jcs2020020
46. E. S. Abdul Rashid, N. Muhd Julkapli, W. A. Yehye. Nanocellulose reinforced as green agent in polymer matrix composites applications. *Polym. Adv. Technol.* **2018**, *29*, 1531. https://doi.org/10.1002/pat.4264
47. A. Abdel-Hakim, A. E. A. A. El-Wakil, S. El-Mogy, S. Halim. Effect of fiber coating on the mechanical performance, water absorption and biodegradability of sisal fiber/natural rubber composite. *Polym. Int.* **2021**, *70*, 1356. https://doi.org/10.1002/pi.6207
48. P. Sahu, M. K. Gupta. Water absorption behavior of cellulosic fibres polymer composites: A review on its effects and remedies. *Journal of Industrial Textiles*. **2022**, *51*, 7480S. https://doi.org/10.1177/1528083720974424
49. A. A. Bachchan, P. P. Das, V. Chaudhary. Effect of moisture absorption on the properties of natural fiber reinforced polymer composites: A review. *Mater. Today Proc.* **2022**, *49*, 3403. https://doi.org/10.1016/j.matpr.2021.02.812
50. N. Lakshmaiya, T. Raja, D. Yuvarajan. Effect of silane-treated jute/sisal cellulose reinforcement on the mechanical, tribological, and hydrophobic behavior of polyester composites. *Clean. Eng. Technol.* **2025**, *29*, 1. https://doi.org/10.1016/j.clet.2025.101122
51. S. Mayakannan, J. B. Raj, V. L. Raja, M. Nagaraj. Effectiveness of silicon nanoparticles on the mechanical, wear, and physical characteristics of PALF/sisal fiber–based polymer hybrid nanocomposites. *Biomass Convers. Biorefin.* **2023**, *13*, 13291. https://doi.org/10.1007/s13399-023-04654-3
52. X. Lu, M. Q. Zhang, M. Z. Rong, D. L. Yue, G. C. Yang. Environmental degradability of self-reinforced composites made from sisal. *Compos. Sci. Technol.* **2004**, *64*, 1301. https://doi.org/10.1016/j.compscitech.2003.10.013
53. M. Y. Kassa, S. T. Mekonone, T. G. Ayaliew, R. G. Rengiah, L. F. Demisie. Optimization of process parameters for sisal fiber-reinforced cornstarch biocomposites in sustainable packaging applications. *Discover Applied Sciences*. **2025**, *7*, 1. https://doi.org/10.1007/s42452-025-07555-4
54. K. Arunprasath, P. Senthamaraikannan, I. Suyambulingam, S. Akash, S. Kathic, M. Vimal Chanth, N. Sunesh, R. Kumar. From degradation to durability: strategies for prolonging the shelf life of natural fiber Composites–A comprehensive review. *Journal of Natural Fibers*. **2025,** *22*, 1. https://doi.org/10.1080/15440478.2025.2554897
55. E. Moll, P. A. V. Freitas, A. Chiralt. Effect of active rice straw extracts on the properties and migration of PHBV films. Food Packaging and Shelf Life. **2025**, *48*, 1. https://doi.org/10.1016/j.fpsl.2025.101454
56. S. Paudel, S. Janaswamy. Use of alfalfa cellulose for formulation of strong, biodegradable film to extend the shelf life of strawberries. International Journal of Biological Macromolecules. **2025**, *290*, 1. https://doi.org/10.1016/j.ijbiomac.2024.139004
57. S. Arif, R. Nadeem, K. Shahzadi, S. Siddique, M. S. Anwar. Synthesis and characterization of ZnO and Zn0.9TM0.1O (TM = Cu and Co) nanoparticles to enhance the shelf life of jujubes and green chilies. **2025**, *131*, 1. https://doi.org/10.1007/s00339-025-08286-4